Journal of Materials Chemistry A

Discovery of a high-pressure phase of rutile-like CoO2 and its potential as a cathode material

Journal:	*Journal of Materials Chemistry A*
Manuscript ID	TA-ART-06-2018-005840.R1
Article Type:	Paper
Date Submitted by the Author:	27-Jul-2018

Complete List of Authors:	Wang, Shuo; Peking University, Materials Science and Engineering Liu, Junyi; Peking University, Qie, Yu; Peking University Gong, Sheng; Peking University, Department of Materials Science and Engineering Sun, Qiang; Peking University, Jena, Purusottam; Virginia Commonwealth University, Physics Department

Discovery of a high-pressure phase of rutile-like CoO_2 and its potential as a cathode material

Shuo Wang[a], Junyi Liu[a], Yu Qie[a], Sheng Gong[a] and Qiang Sun[a,b,c,*], Puru Jena[c]

[a]Department of Materials Science and Engineering, College of Engineering, Peking University, Beijing 100871, China

[b]Center for Applied Physics and Technology, Peking University, Beijing 100871, China

[c]Department of Physics, Virginia Commonwealth University, Richmond, VA 23284, USA

Abstract

Due to the structure failure of CoO_2 layered geometry, there has been considerable efforts to improve the reversible capacity of commercial $LiCoO_2$ cathode material. Using a global structure search, we have discovered a rutile-like CoO_2 phase as the ground state at 50 GPa. The material is thermally, mechanically and dynamically stable, even after removing the pressure. We show that, when lithiated, this $LiCoO_2$ material can serve as an improved cathode material for Li-ion battery. Its many advantages include good structure stability against transition metal migration and oxygen loss, one-dimensional channels for Li ion diffusion with variable energy barriers (0.36~0.86 eV), enhanced ionic mobility, and good intrinsic electronic conductivity brought about by its metallic band structure. Furthermore, with a voltage platform of 3.2~3.8V, it provides better stability against conventional carbonate solvents than conventional layered cathode materials (> 4.0V). All these features demonstrate that the non-layered CoO_2 phase synthesized at high pressure would be a promising cathode material, going beyond the currently used layered phase.

Keywords: Cathode material, $LiCoO_2$, High pressure, DFT calculations

Introduction

Layered lithium transition metal (TM) oxides $LiMO_2$ (M=Co, Ni, Mn, etc.)[1-3] are among the most widely used cathode materials in commercial Li-ion batteries (LiBs). In particular, $LiCoO_2$, introduced by Goodenough and Mizushima[4] in 1980s, shows great electrochemical performance, such as high specific capacity, high voltage, low over-potential and good reversibility[5]. But in practical operations only 50% (~140 mAh/g)[6, 7] of the theoretical capacity (273 mAh/g) could be reached in $LiCoO_2$/C Li-ion cells. This is because of the strong repulsion[8] between CoO_2 layers and metastable "Li–Co dumbbell" intermediate[9] that occurs in the absence of Li atoms. This leads to phase transition, oxygen release, and structure failure. Scientists and engineers have made numerous efforts to push this limit further via chemical substitution, composite structure and so on, aiming to stabilize the delithiated layered framework[10-12]. As a result, many modified and optimized cathode materials have been developed by using layered-structure with improved capacity (>170mAh/g) such as NCA ($LiNi_xCo_yAl_{1-x-y}O_2$)[13], NCM ($LiNi_xCoyMn_{1-x-y}O_2$)[14], and $[LiCoO_2]_x/[Li_2MnO_3]_{1-x}$ composite [15]. However, the fundamental problem of instability of delithiated layered structure has never been solved and reversible theoretical capacity is still not achieved.

To go beyond such a limitation, it is necessary to develop new cathode materials to maximize the reversible capacity. Cobalt usually shows +2 or +3 valence in oxides such as Co_3O_4, Co_2O_3 and CoO; however, it seldom shows +4 valence state except in layered CoO_2 obtained by de-intercalation of Li_xCoO_2 phases. In this paper, we follow a different strategy and explore the merit of high-pressure synthesis. Note that high pressure is an effective way to change atomic bonding features because it can overcome the chemical reactive barrier[16], change interatomic distances and bonding patterns[17], reorder the atomic orbitals[18], and induce structural phase transitions[19]. Thus, synthesizing materials under high pressure could make the impossible possible! A classic example is graphite vs diamond; at high pressure, stable graphite turns into metastable diamond by reversing the energetic order of these two carbon allotropes. Other examples include H_3S with superconducting temperature of 203K at 155 GPa[20], super-hard nano-twinned diamond with Vickers hardness of 200 GPa[21], high-energy-density cg-N above 110 GPa[22] (single-bond cubic form of nitrogen), etc. In these successful cases, first-principles calculation and structure prediction methods have played a key role, providing guidance for experimental explorations.

Encouraged by these advances, we explore the possibility of achieving a new delithiated

cathode material CoO_2 phase that is stable at high pressure. Using density functional theory combined with global structure search, we discover a rutile-like CoO_2 phase to be the ground state at 50GPa. Equally important, it remains stable dynamically and thermally, even after pressure is removed. Compared to the layered-structure $LiCoO_2$, the new phase is more stable against oxygen release as well as TM displacement. Further, it has metallic band structure with desirable charging/discharging voltage platform, moderate ionic diffusion barriers and enhanced ionic mobility. In addition, the intrinsic stability and considerable ionic diffusivity in the delithiated sample provides improvement in energy density over traditional cathode materials. The results reinforce the great merit of exploring new cathode materials using high-pressure synthesis techniques.

Methods

Using the CALYPSO (Crystal structure AnaLYsis by Particle Swarm Optimization) structure prediction package[23] and density functional theory (DFT) as implemented in the Vienna Ab Initio Simulation Package (VASP)[24] we perform global structure search at high pressure for stable/metastable structures of given chemical composition (e.g. CoO_2). To simulate actual battery operating environment, pressure is removed in subsequent calculations. Projector augmented-wave (PAW) method[25], Perdew–Burke–Ernzerhof (PBE)[26] generalized-gradient approximation (GGA) for exchange and correlation potential, and GGA+U scheme (with a U of 4.91 eV for Co^{3+}/ Co^{4+}) [27] are used. The structure is relaxed without symmetric restraint using conjugated gradient method. The convergence criteria for total energy and Hellmann-Feynman force are set to 1×10^{-4} eV, and 1.0×10^{-2} eV/Å, respectively. The electronic density of states is calculated by employing a 10×11×15 Monkhorst-Pack k-point grid[28]. More accurate band structure is also calculated using the Heyd–Scuseria–Ernzerhof (HSE06)[29] functional. The dynamical stability is verified by calculating the vibrational spectra using finite displacement approach as implemented in the Phonopy code[30]. The thermodynamic stability is confirmed with *ab intio* molecular dynamic (AIMD) simulation in canonical (NVT) ensemble using the Nose-Hoover heat bath scheme (500K) in a 3×3×3 supercell. Finite difference method[31] is used to calculate the Hessian matrix. The mechanical stability is proved using the criteria for orthorhombic phase[32].

Diffusion barriers are calculated using the climbing image-nudged elastic band (CI-NEB) method[33] with a 2×2×4 supercell, while lattice vectors are fixed to the defect-free relaxed parameters.

Furthermore, AIMD simulations lasting for 20 ps at temperatures from 700K to 2500K are carried out in fixed lattice to study Li-ion transport. Elevated temperatures are used to speed up the ion-hopping process. The mean square displacement (MSD) is calculated as shown below[34]

$$\langle[\vec{r}(t)]^2\rangle = \frac{1}{N}\sum_{i=1}^{N}\langle[\vec{r_i}(t+t_0) - \vec{r_i}(t_0)]^2\rangle \qquad (1)$$

where $\vec{r}(t)$ is the displacement of the ith Li^+ ion at time t and N is the total number of Li^+ ions in the system. The diffusion coefficient (*D*) at each temperature is calculated by fitting to the MSD according to

$$D = \lim_{t\to\infty}\left[\frac{1}{2dt}\langle[\vec{r}(t)]^2\rangle\right], \qquad (2)$$

where *d* is the dimensionality of diffusion and *t* is the elapsed simulation time. From the Nernst-Einstein relation, the conductivity (σ) can be calculated as

$$\sigma = D\frac{Ne^2}{kT} \qquad (3)$$

N is the number of ion pairs per cm^3; other symbols have their customary meaning. The activation energy E_a is obtained by using the Arrhenius model

$$\sigma = \frac{A}{T}exp\left(\frac{E_a}{kT}\right) \qquad (4)$$

Here, A is the constant fitting parameter for a specified crystal lattice.

In order to find the most energy-favorable configuration at different Li concentration, we use the cluster expansion (CE) method to describe the configurational energy. All structures are fully relaxed in the CE calculation to determine stable intermediate configurations. In our work, the Li_xCoO_2 is taken as an alloy system and each possible Li site *i* is represented by an occupation variable σ_i, which takes the value 1 if Li resides at that site and −1 if a vacancy is at that site. The configuration-dependent Hamiltonian can be mapped onto a generalized Ising Hamiltonian:

$$E(\sigma) = \mathrm{J}_0 + \sum_i J_i\sigma_i + \sum_{j<i} J_{ij}\sigma_i\sigma_j + \sum_{k<j<i} J_{ijk}\sigma_{ijk} + \ldots = \mathrm{J}_0 + \sum_\alpha J_\alpha\varphi_\alpha \qquad (5)$$

Here the subscript *i, j*, and *k* range over all occupation sites, φ_α is the product of occupation variables σ_i, $\sigma_j \ldots \sigma_k$ that form a cluster α, which can be a single point, a pair cluster, a triple cluster, etc. J_α is the corresponding effective cluster interaction whose value converges to zero as the size or distance between the clusters increases. This is obtained by fitting them to the energies of selected configurations calculated from first-principles. The fitted CE quality is measured by the cross-validation (CV) score, and the fitting process are carried out via Alloy Theoretic Automated Toolkit

(ATAT) code[35].

Results and discussions

1. Structural stability and electronic properties

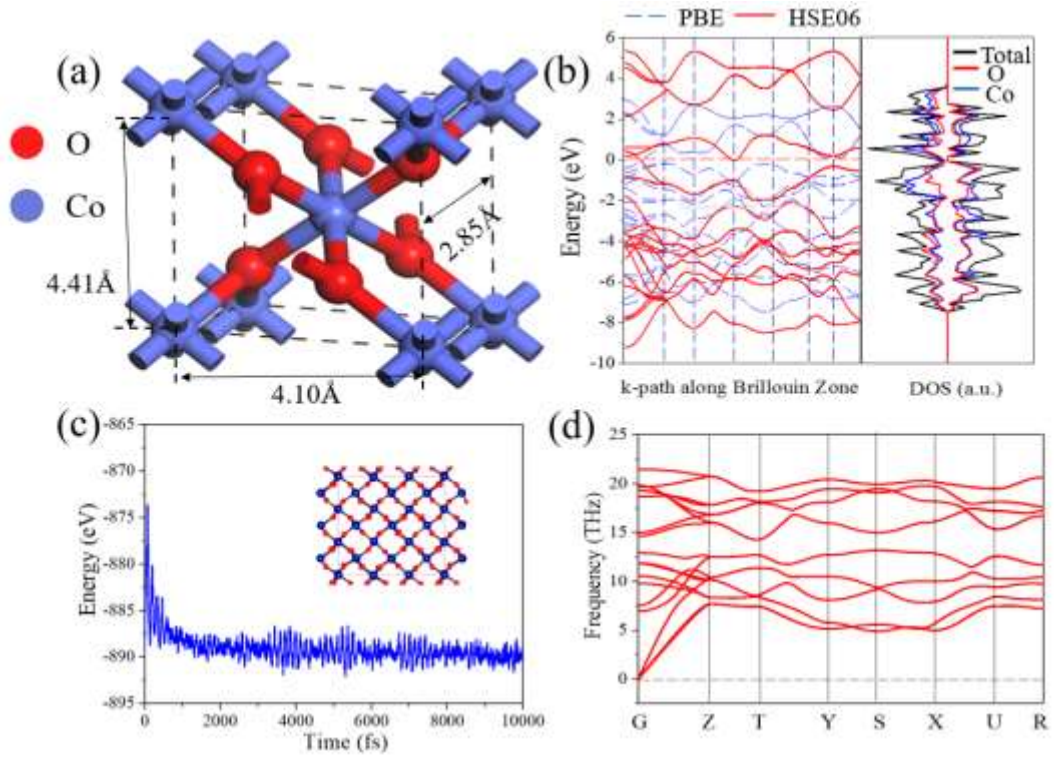

Figure 1. (a) Crystal structure, (b) Band structures and partial density of states calculated using PBE and HSE06 functional, (c) AIMD Energy fluctuation as a function of time at 500K, (d) Phonon dispersion of rutile-like CoO_2.

We perform global structural search of CoO_2 at 50 GPa, which yielded the ground-state structure to be similar to that of rutile TiO_2. However, compared to the standard-rutile structure, we find distortion in the structure of CoO_2 with symmetry changing from *P42/mnm* to *Pnnm*. To confirm the origin of this distortion, we calculated the phonon spectra for standard rutile CoO_2 at vacuum and at 50GPa. The results are shown in Figure S1(a), where the imaginary frequencies exist at both vacuum and high pressure, suggesting the instability of the regular rutile-type CoO_2. The imaginary phonon with low frequency comes from the rotation of Co-O octahedrons around the octahedral center. Because of the different electronic distribution between Ti ($3d^24s^2$) and Co($3d^74s^2$), the octahedrons in CoO_2 are not regular as those in TiO_2. The percentage deviation between long and short lattice edges is used as a reference to measure the level of distortion. Pressure dependence of

the distortion is plotted in Figure S1(b), showing that the distortions first get enhanced quickly with increasing pressure and then slow down at high pressure. All these results prove that the distortion is necessary for the stabilization of rutile-like CoO_2 at high pressure. Further, this structure remains intact even after the pressure is removed, as shown in Figure1 (a). Here, Co and O occupy 2a and 4g sites, respectively. Details of lattice parameters and atomic coordinates are given in Table S1. To explore the effect of pressure on materials, pressure dependence of enthalpy curves with respect to the experimental delithiated Li_xCoO_2 is calculated (Figure S2). We find the ground-state energy to reverse with increasing pressure to 7 GPa, implying a possible phase transition. This suggests that it is highly feasible to synthesize a rutile-like CoO_2 phase by compression. This is also confirmed by calculating the formation energy of CoO_2, as shown below:

$$\mathrm{Co(s)} + \mathrm{O_2}(g) \rightarrow CoO_2(s) \qquad (6)$$

$$\Delta H = E_{CoO_2(s)} - E_{\mathrm{O_2}(g)} - E_{\mathrm{Co(s)}} \qquad (7)$$

Here, *E* is the total energy per f.u. Because the accurate energy of O_2 is difficult to calculate directly due to the overestimated binding effect of O_2 molecule in DFT-GGA calculation[36], we obtain the energy of O_2 molecule using the following equation:

$$E(O_2) = 2E_{DFT}(\mathrm{H_2O}) - 2E_{DFT}(\mathrm{H_2}) - 2\Delta E_{exp}(\mathrm{H_2O}) \qquad (8)$$

The formation energy is found to be -2.51 eV, which means that the chemical reaction can take place. Because oxygen release has always been a critical problem during deep delithiation, we study oxygen stability by exploring the possibility of oxygen loss in the following process,

$$CoO_2(s) \rightarrow CoO_{2-y}(s) + \frac{y}{2}O_2(g) \quad (9)$$

We calculate the resulting change of enthalpy as

$$\Delta H = \frac{CoO_{2-y}(s) + (y/2)E_{O_2} - CoO_2(s)}{y/2} \qquad (10)$$

The value is found to be +0.21eV, which suggests that oxygen-release reaction is energetically unfavorable, even under full delithiated condition. In addition, we simulate the formation of oxygen-dimer between adjacent O atoms in layered and rutile-like structure, respectively. After optimization, we see from Figure S3 that Co is displaced and oxygen-dimer remains in layered $LiCoO_2$. For rutile-like structure, the displaced O atoms reset themselves and primary framework is recovered. Furthermore, the AIMD simulation at 1500K is conducted to compare the relative stability between layered and rutile-like structures; the results are shown in Figure S4. Oxygen release and Co

migration occur in layered structure within 200fs while rutile-like framework withstands thermal disturbance without formation of oxygen-dimer and migration of Co, even after 5000fs. We think this is because of the combination of the large interspace and bonding break of O atoms in octahedral coordination in layered structure, which provides the possibility for structural reconstruction. All the above results indicate that rutile-like structure has good stability against oxygen loss.

To examine the thermodynamic stability further, *ab intio* molecular dynamic (AIMD) simulation is carried out in a 3×3×3 supercell at 500K using the canonical ensemble (NVT). Total energy fluctuation as a function of time is plotted in Figure 1(c). In the inset, we present the geometry after ten-picosecond relaxation. The average total potential remains nearly constant and no structural reconstruction occurs, confirming that rutile CoO_2 is thermally stable. To verify its dynamical stability, we calculated the phonon frequencies; the results are shown in Figure 1(d). Note that there is no imaginary mode in the vibrational spectra in the entire Brillouin zone, which shows that the rutile CoO_2 is dynamically stable. Besides, the mechanical stability is also established according to the criteria of orthorhombic phase[37]:

$$C_{11}>0,\ C_{22}>0,\ C_{33}>0,\ C_{44}>0,\ C_{55}>0,\ C_{66}>0,$$

$$[C_{11}+C_{22}+C_{33}+2(C_{12}+C_{13}+C_{23})]>0,$$

$$(C_{11}+C_{22}-2C_{12})>0,\ (C_{22}+C_{33}-2C_{23})>0,\ (C_{11}+C_{33}-2C_{13})>0 \qquad (11)$$

The detailed values of C_{xy} are listed in Table S2. Clearly, they satisfy the mechanical stability criteria, and rutile CoO_2 phase is also mechanically stable. Using Voigt-Reuss-Hill approximation, the bulk modulus (B) and shear modulus (G) of CoO_2 are also calculated. The results are listed in Table 1. One can see that the *Pnnm* CoO_2 phase shows comparable mechanical properties with those of standard-rutile TiO_2, which has been found to have desirable mechanical stability[38] when used as anode in Li/Na ion battery.

For a cathode material, a crucial property is electronic conductivity. For example, practical application of phosphates ($LiFePO_4$) is held back due to its low intrinsic electronic and ionic conductivity. To further understand the electronic properties of the studied system, we calculate the band structure and partial density of states (DOS) of rutile CoO_2 using GGA+U (U=4.91 eV) level of theory. The results are given in Fig 1(b). Different from semi-conducting rutile TiO_2, the rutile-like CoO_2 is metallic with O 2p-orbital and Co 3d-orbital crossing the Fermi level. Such metallic transition was also seen in our previous work on high-pressure Li_2MnO_3 phase[39]. Because pressure

usually reduces interatomic distances and consequently enhances atomic interactions, the energy bands are broadened at high pressure. The resulting band overlap will often induce insulator-to-metal or semiconductor-to-metal transition. Such intrinsic metallicity would improve the electronic response during the charging/discharging process. More accurate band structure calculations using the HSE06 functional authenticates the metallicity of rutile-like CoO_2.

Table1. Bulk modulus (B), shear modulus (G), Young's modulus (E) in GPa and Possion's ratio (ν) of CoO_2 and TiO_2. Subscript V denotes the Voigt bound, R denotes the Reuss bound, H denotes the Hill average.

Materials	Symmetry	B_V	B_R	G_V	G_R	B_H	G_H	E	ν
CoO_2	*Pnnm*	194	142	130	83	168	107	265	0.23
TiO_2	*P42/mnm*	214	204	123	96	209	110	280	0.28

2. Li-ion storage and ionic mobility

Due to the different chemical bonding characteristics between Co and Ti, the one-dimensional channels in rutile-like CoO_2, as shown in Figure 4(c), are not rectangular as those in rutile TiO_2. The Li atom tends to be at the central position of the one-dimensional channels where energy is lower and steric hindrance is smaller. After all the optimal sites are occupied, the insertion of additional Li atoms would cause positive binding energy, which means half-cell lithiation reaction cannot go on spontaneously because of the strong repulsive interaction between Li ions. The chemical formula ends up with $LiCoO_2$ after full lithiation, leading to a theoretical capacity of 273 mAh/g. After lithiation, we find the crystal lattice to expand along the *x* (from 4.41 Å to 4.68 Å) and *y* (from 4.10 Å to 4.67 Å) axes, but remains nearly intact along the *z* direction. To verify the mechanical stability of the CoO_2 frameworks during lithiation/delithiation process, we calculated the compressive and tensile stress (σ) as a function of uniaxial strain along the *x* and *y* directions and plot the results in Figure 3. The stress shows an approximate linear growth with increasing compressive and tensile strains along both *x* and *y* directions, indicating that the rutile CoO_2 framework can sustain the strain caused by the volume change during charging/discharging process, thus preventing mechanical failure.

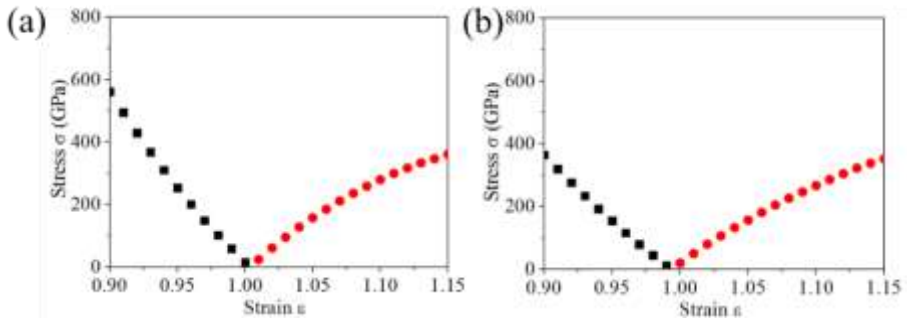

Figure 2. Compressive and tensile stress σ as a function of uniaxial strain along the (a) *x*, (B) *y* direction, respectively.

Based on the lithiated configuration, the Li migration energy barriers are calculated using CI-NEB. The corresponding results and diagrammatic sketches are shown in Figure 3. Li ions, shuttling between the channels, have much higher barrier (>3eV) than that of diffusion along the channels. The diffusion coefficient (*D*) can be evaluated by using equations (3) and (4). Based on the barrier difference, the mobility of Li within the one-dimensional channel is at least 5.5×10^{34} higher than that of ionic diffusion between channels at room temperature. Therefore, we expect that the Li ions should show one-dimensional mobile behavior. This expectation is also confirmed in the following AIMD calculation.

To simulate the Li ion diffusion, mono-vacancy is usually used. However, the distribution and concentration of vacancies can impact on ionic motion as found in sodium-ion diffusion in layered P2 and P3 oxides[40]. In the actual charging process, more vacancies are introduced which would lead to vacancy clustering because Li ionic movements in the one-dimensional diffusion channels may lag behind. To simulate such situation, we adopt a tri-vacancy model. The energy barrier for single atom diffusion is 0.79eV. The ionic diffusion barrier is similar (0.86 eV) in mono-vacancy model but different from 0.36 eV in tri-vacancy model. Our results are comparable to those of layered-structure lithium metal oxides such as Li_xCoO_2 (0.36~0.76 eV), Li_xAlO_2 (0.65~1.41 eV), Li_xMnO_3 (0.51~0.84 eV), $LiNi_xMn_yCo_{1-x-y}O_2$ (NMC, 0.75~0.90 eV) etc. For a better understanding of the underlying reasons for different ionic diffusion behavior in mono-vacancy and tri-vacancy model, we highlight three points here: 1) there is less steric hindrance and ionic repulsive interaction as more vacancies are introduced. At the initial and final state, we have observed the mobile Li ion deviating from the original position and getting closer to the mono vacancy to reduce repulsive interaction with adjacent Li ions. Hence, the migration distance is different in the mono-vacancy

and tri-vacancy model. 2) The potential energy landscape near the optimal adsorption site is flat, as shown in CI-NEB results. This results from the competition between increased interaction with more coordinated sites and weakened binding effect due to elongated Li-O bonds. 3) Strain induced by Li insertion. When only one vacancy is introduced into lithiated CoO_2 supercell, the bottleneck of one-dimensional channel tends to shrink locally to release the strain induced by Li insertion, suggesting that the diffusing atom has to overcome local stress. Combined with the valley of the potential surface in mono-vacancy model, it becomes harder for diffusing Li ion to pass through. On the contrary, the release of stress would be well distributed when more vacancies are introduced, hence the potential energy surface would become smoother than that in the mono-vacancy model. This in turn would enhance ionic mobility.

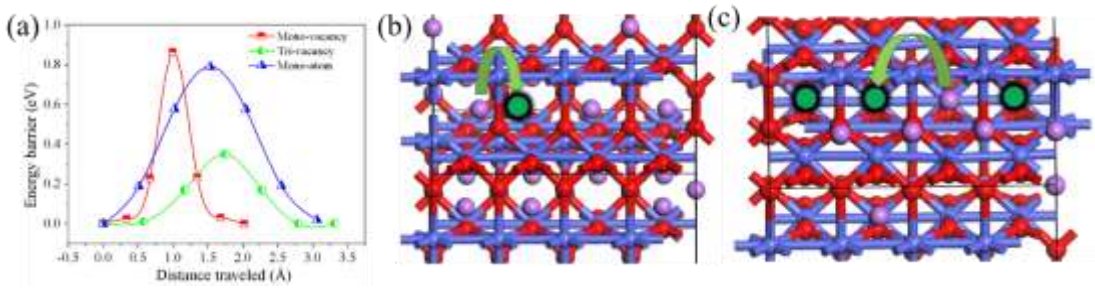

Figure 3. (a) Migration energy barriers in rutile-like CoO_2, and illustration of the lithium migration associated with (b) mono-vacancy and (c) tri-vacancy. The vacancy, Li, O, Co atoms and vacancy-clusters are marked with green, purple, red, blue and green, respectively.

To explore the ionic diffusion behavior further from the perspective of thermo-kinetics, we carry out AIMD simulation from 700K to 2500K in a 2×2×4 supercell with four Li vacancies present. We use elevated temperature to accelerate the diffusion process, which was thermalized over 4-ps with a time-step of 2 fs. The corresponding results are illustrated in Figure 4. In practice, convergence of *D* can be achieved within 20 ps due to the fast ionic processes in the simulated materials. No structure failure is observed during the simulation. The Li ions do not show consecutive ionic diffusion behavior until the temperature rises above 1500K. The AIMD simulations in layered-structure are also carried out with the same parameters as in four vacancies introduced in a 3×3×4 supercell. The results are shown in Figure S5. Based on the fitting to the Arrhenius model, the calculated diffusion coefficient at 2000K is $1.38\times10^{-5}cm^2/s$ for layered

structure and $1.50\times10^{-5}cm^2/s$ for rutile-like structure, while at 500K the corresponding values are 6.7×10^{-12} and $1.05\times10^{-11}cm^2/s$, respectively. Thus, the ionic conductivity of the rutile-like CoO_2 is similar to that of the layered structure. This means that rutile-like CoO_2 can serve as a cathode material. Based on the AIMD simulation, activation enthalpy can be deduced from the Arrhenius relation $D \propto exp(-E_a/k_BT)$. Figure 4(b) only shows the Arrhenius plot for different diffusion coefficients from 1500 to 2500 K, because no consecutive ionic diffusion was observed when temperature is below 1000K. In our fitting, the standard errors of intercept and slope are 3.2% and 3.5%, respectively. The calculated diffusion energy barrier (0.88 eV) is consistent with the CI-NED result (0.86 eV) in the mono-vacancy model. To visualize the ionic migration channels, Li diffusion trajectories at 1500K are shown in Figure 4(c). We note that the Li ion trajectories only overlap along the z direction and no hopping between different channels is seen. Figure 4(d) shows the statistical results of MSD_{Li} along different directions, consecutive ionic diffusion only occurs along the *z* direction, but not for *x* and *y* direction. All these results confirm that ionic conductivity in rutile-like CoO_2 is one-dimensional. Besides, the model with higher vacancy concentration ($Li_{0.5}CoO_2$) is also considered. Enhanced ionic mobility is observed in Figure S6. The Li diffusion coefficient at 1500K is six times larger than that of layered-structure $LiCoO_2$, with low-concentration carriers at 2000K.

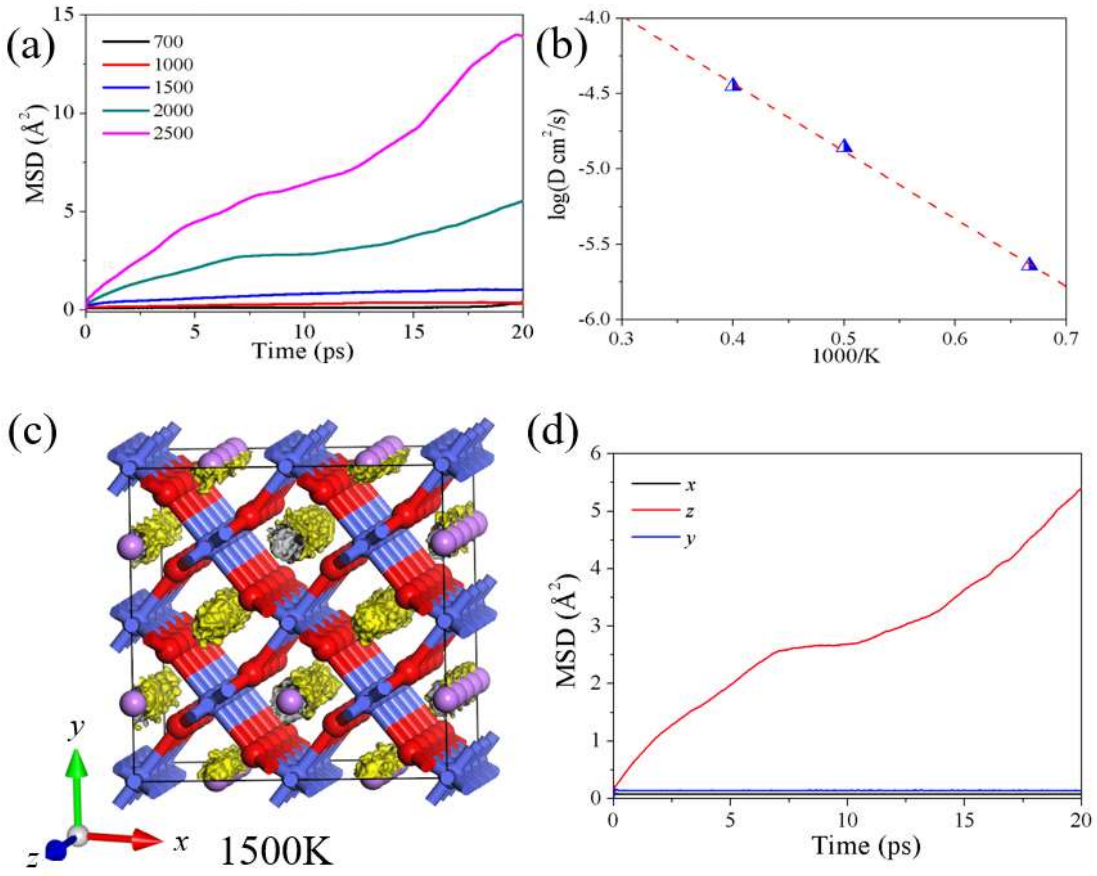

Figure 4. (a) MSD_{Li} as a function of MD simulation time at different temperatures. (b) Fitting to the Arrhenius model. (c) Projection of Li trajectories (yellow) and (d) MSDLi along different directions at 1500 K. O (red), Li (purple), and Co (blue) atoms remain at their initial position

3. Charge/discharge voltage curve

Open-circuit voltage, which varies with the Li concentration, is another key factor for characterizing the performance of the Li-ion battery. For rutile-like CoO_2, the charge/discharge process follows the common half-cell reaction vs. Li/Li+:

$$(x_2 - x_1)\mathrm{Li}^+ + (x_1 - x_2)\mathrm{e}^- + \mathrm{Li}_{X1}CoO_2 \leftrightarrow \mathrm{Li}_{X2}CoO_2 \qquad (12)$$

The influence of volume, pressure, and entropy is ignored here. The average voltage in the concentration range of $x_1 < x < x_2$ is estimated by calculating the energy difference over parts of the Li composition domain:

$$V \approx \frac{E_{Lix_1C_oO_2} - E_{Lix_2C_oO_2} + (x_2 - x_1)E_{Li}}{x_2 - x_1} \qquad (13)$$

To predict the charge/discharge voltage platform accurately, we first need to confirm the most stable Li configuration at different intermediate Li concentration. Cluster expansion is an efficient method

to predict the formation energy for substitutional systems[41], for electrode materials such as Li_x-graphite, layered-structure Li_xCoO_2, etc[42, 43], and has been successfully applied to many alloy systems such as $Co_{2-x}Mn_{1+x}Si$[44], V–Ta alloy[45] and vacancies in ordered and disordered $Al_{1-x}Li_x$[46] etc. Recently, it has been applied to Li-ion electrodes for determining the intermediate phase, including $Li_{1-x}CoO_2$ [7], $Li_{2-x}MnO_3$[47], Li_x-bco-C16[48], etc. Based on these demonstrated successes, we have used it to predict the intermediate states. The Hamiltonian for Li_xCoO_2 is constructed by fitting the energies calculated for 107 configurations with the simulation cell sizes up to 40 atoms/cell, and the fitting cross-validation (CV) score is 21 meV/formula, less than the typical value of 25 meV. For a given Li-vacancy arrangement, the formation energy is defined as follows:

$$E_f(\sigma) = E_{LixCoO2} - (1-x)E_{CoO2} - xE_{LiCoO2} \qquad (14)$$

which is used to estimate the relative stability of specific Li_xCoO_2 configuration with respect to phase separated xLiCoO$_2$ and (*1-x*)CoO$_2$. The CE fitting results at different Li concentration are shown in Figure 5. Three stable configurations at intermediate concentration (x = 0.10, 0.17, 0.5) are found and the corresponding structures are shown in Fig S7. The Li ions still resides in the vicinity of the optimal adsorption sites in all intermediate phases. Because the voltage profile can be deduced from the formation energy, which in turn can be affected by different U, we used two values of U, namely, 4.91 and 3.30 eV. The former is used for Co^{3+}/ Co^{4+} in layered $LiCoO_2$ which agrees well with the experiment[49] for the voltage profile. The latter value is used by fitting to the experimental oxidation energies of cobalt oxides[50]. The open-circuit voltage curve is presented in Figure 5(b). The voltage rises with increasing delithiation and four voltage regions are displayed. The average voltage is 3.7V for U=4.91, which is slightly less than the calculated value (4.0~4.2V) by Zhou et.al[51] using the same U for layered-structure. For U=3.30, the maximum voltage is less than 3.5V. The results show that rutile-like CoO_2 may provide better safety due to the stability of conventional carbonate solvents at low voltage (<4V)[52]. Since the energy density is determined by the integral of voltage and reversible capacity, when combining intrinsic deep-delithiation stability with appropriate voltage platform, the rutile-like CoO_2 might show improved energy density as cathode over the traditional layered-structure.

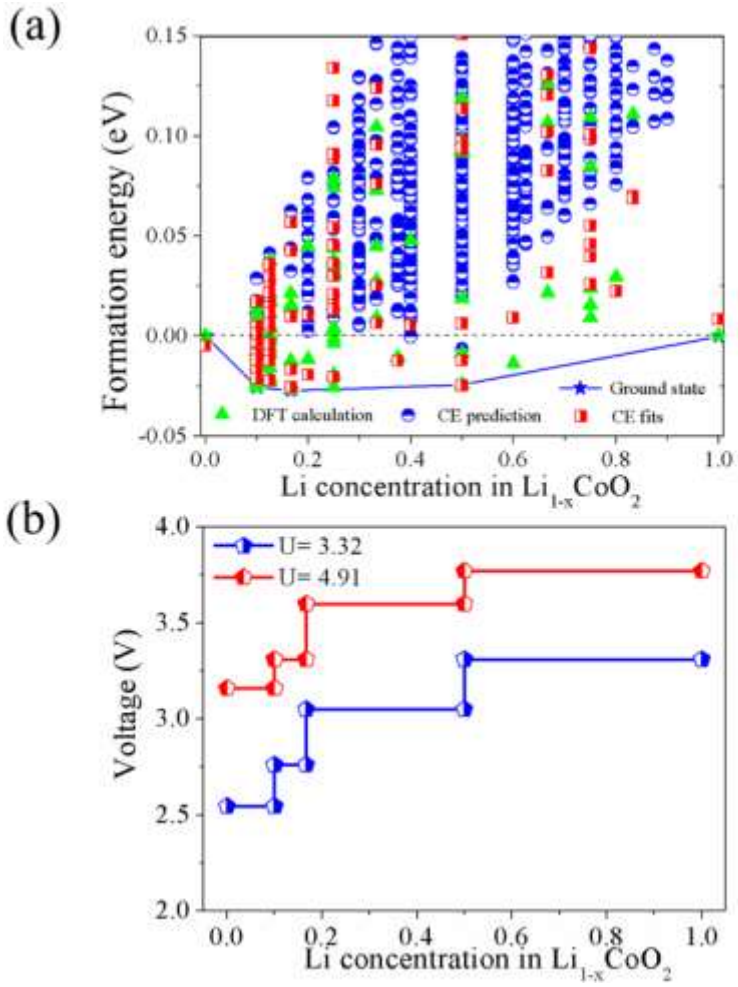

Figure 5. (a) Formation energies predicted by CE method for the 107 different Li configurations with three stable intermediate phases and (b) corresponding voltage profile with different U value (red/blue for 4.91/3.32) along the minimum energy path.

Conclusions

In this work, using global crystal structure search method combined with first-principle calculations, we have identified a stable delithiated high-pressure phase of CoO_2. This rutile-like CoO_2 is found to be the ground state at 50 GPa and remains stable dynamically, thermally and mechanically even after pressure is removed. We have studied the potential of this rutile $LiCoO_2$ as a cathode material for Li-ion battery. We find it to have the following advantages over the conventional layered structure: (1) Better structure stability against oxygen loss and TM displacement than the layered structure, (2) good mechanical strength to endure volume expansion during charging/discharging process, (3) one-dimensional diffusion channels for Li ions with preferred energy barriers (0.36~0.86 eV) and enhanced ionic mobility, (4) a good electronic

conductivity due to the intrinsic metallic band structure, and (5) an improved safety against conventional carbonate solvents due to the appropriate average voltage platform (3.2~3.8V). We hope that these encouraging results will stimulate further theoretical and experimental effort to develop novel cathode materials using high-pressure synthesis.

ACKNOWLEDGMENTS: This work is partially supported by grants from the National Key Research and Development Program of China (2016YFB0100200), and from the National Natural Science Foundation of China (21573008 and 21773003). P. J. acknowledges the support by the U.S DOE, Office of Basic Energy Sciences, Division of Material Sciences and Engineering under Award No. DE-FG02-96ER45579. Part of the numerical simulations are performed on the High-Performance Computing Platform of Peking University and High-performance Computing Platform of CAPT.

References:

1. Wang, Y.; Cao, G., Developments in Nanostructured Cathode Materials for High‐Performance Lithium‐Ion Batteries. *Advanced Materials* **2010,** 39, (37), no-no.
2. Ceder, G.; Chiang, Y. M.; Sadoway, D. R.; Aydinol, M. K.; Jang, Y. I.; Huang, B., Identification of cathode materials for lithium batteries guided by first-principles calculations. *Nature* **1998,** 392, (6677), 694-696.
3. Fergus, J. W., Recent developments in cathode materials for lithium ion batteries. *Journal of Power Sources* **2010,** 195, (4), 939-954.
4. Mizushima, K.; Jones, P. C.; Wiseman, P. J.; Goodenough, J. B., Li x CoO 2 (0<x<-1): A new cathode material for batteries of high energy density. *Materials Research Bulletin* **1980,** 15, (6), 783-789.
5. Yoshino, A.; Takizawa, Y.; Koyama, A.; Inoue, K.; Yamashita, M.; Minato, Y.; Kuribayashi, I., Secondary battery. In US: 1997.
6. Komaba, S.; Murata, W.; Ishikawa, T.; Yabuuchi, N.; Ozeki, T.; Nakayama, T.; Ogata, A.; Gotoh, K.; Fujiwara, K., Electrochemical Na Insertion and Solid Electrolyte Interphase for Hard‐Carbon Electrodes and Application to Na‐Ion Batteries. *Advanced Functional Materials* **2011,** 21, (20), 3859‐3867.
7. Ven, A. V. D.; Aydinol, M. K.; Ceder, G.; Kresse, G.; Hafner, J., First-principles investigation of phase stability in LixCoO2. *Physical Review B* **1998,** 58, (6), 2975-2987.
8. Rozier, P.; Tarascon, J. M., Review—Li-Rich Layered Oxide Cathodes for Next-Generation Li-Ion Batteries: Chances and Challenges. *Journal of The Electrochemical Society* **2015,** 162, (14), A2490-A2499.
9. Zhang, T.; Li, D.; Tao, Z.; Chen, J., Understanding electrode materials of rechargeable lithium batteries via DFT calculations. *Progress in Natural Science: Materials International* **2013,** 23, (3), 256-272.
10. Wu, E. J.; Tepesch, P. D.; Ceder, G., Size and charge effects on the structural stability of LiMO2 (M = transition metal) compounds. *Philosophical Magazine Part B* **1998,** 77, (4), 1039-1047.

11. Yu, H.; Zhou, H., High-Energy Cathode Materials (Li2MnO3-LiMO2) for Lithium-Ion Batteries. *Journal of Physical Chemistry Letters* **2013,** 4, (8), 1268.

12. Jun, L.; Qing, P.; Weiyang, W.; Caiyun, N.; Lihong, L.; Yadong, L., Nanoscale Coating of LiMO2 (M = Ni, Co, Mn) Nanobelts with Li+-Conductive Li2TiO3: Toward Better Rate Capabilities for Li-Ion Batteries. *Journal of the American Chemical Society* **2013,** 135, (5), 1649.

13. Jeong, G.; Kim, Y. U.; Kim, H.; Kim, Y. J.; Sohn, H. J., Prospective materials and applications for Li secondary batteries. *Energy & Environmental Science* **2011,** 4, (6), 1986-2002.

14. Nitta, N.; Wu, F.; Lee, J. T.; Yushin, G., Li-ion battery materials: present and future. *Materials Today* **2015,** 18, (5), 252-264.

15. Lu, Z.; Zhaohui Chen, A.; Dahn, J. R., Lack of Cation Clustering in Li[NixLi1/3-2x/3Mn2/3-x/3]O2 (0 < x $\leqslant$ 1/2) and Li[CrxLi(1-x)/3Mn(2-2x)/3]O2 (0 < x < 1). *Chemistry of Materials* **2003,** 15, 3214-3220.

16. Zurek, E.; Hoffmann, R.; Ashcroft, N. W.; Oganov, A. R.; Lyakhov, A. O., A little bit of lithium does a lot for hydrogen. *Proceedings of the National Academy of Sciences of the United States of America* **2009,** 106, (42), 17640-3.

17. Yang, G.; Wang, Y.; Peng, F.; Bergara, A.; Ma, Y., Gold as a 6p-element in Dense Lithium Aurides. *Journal of the American Chemical Society* **2016,** 138, (12), 4046.

18. Ma, Y.; Eremets, M.; Oganov, A. R.; Xie, Y.; Trojan, I.; Medvedev, S.; Lyakhov, A. O.; Valle, M.; Prakapenka, V., Transparent dense sodium. *Nature* **2009,** 458, (7235), 182.

19. Miao, M., Cs in high oxidation states and as a p-block element. *Nature Chemistry* **2013,** 5, (10), 846-852.

20. Drozdov, A. P.; Eremets, M. I.; Troyan, I. A.; Ksenofontov, V.; Shylin, S. I., Conventional superconductivity at 203 kelvin at high pressures in the sulfur hydride system. *Nature* **2015,** 525, (7567), 73.

21. Huang, Q.; Yu, D.; Xu, B.; Hu, W.; Ma, Y.; Wang, Y.; Zhao, Z.; Wen, B.; He, J.; Liu, Z., Nanotwinned diamond with unprecedented hardness and stability. *Nature* **2014,** 510, (7504), 250.

22. Mailhiot, C.; Yang, L. H.; Mcmahan, A. K.; Iii, T. W. B., Polymeric nitrogen. *Physical Review B Condensed Matter* **1994,** 46, (22), 14419-14435.

23. Wang, Y.; Lv, J.; Zhu, L.; Ma, Y., Crystal Structure Prediction via Particle Swarm Optimization. *Physics* **2010,** 82, (9), 7174-7182.

24. Kresse, G.; Furthmüller, J., Efficient iterative schemes for ab initio total-energy calculations using a plane-wave basis set. *Physical Review B* **1996,** 54, (16), 11169.

25. Blöchl, P. E., Projector augmented-wave method. *Physical Review B* **1994,** 50, (24), 17953.

26. Perdew, J. P.; Burke, K.; Ernzerhof, M., Generalized gradient approximation made simple. *Physical review letters* **1996,** 77, (18), 3865.

27. Hoang, K.; Johannes, M. D., Defect chemistry in layered transition-metal oxides from screened hybrid density functional calculations. *Journal of Materials Chemistry A* **2014,** 2, (15), 5224-5235.

28. Monkhorst, H. J.; Pack, J. D., Special points for Brillouin-zone integrations. *Physical Review B* **1976,** 13, (12), 5188.

29. Heyd, J., Hybrid functionals based on a screened Coulomb potential. *Journal of Chemical Physics* **2003,** 118, (18), 8207-8215.

30. Togo, A.; Oba, F.; Tanaka, I., First-principles calculations of the ferroelastic transition between rutile-type and CaCl 2-type SiO 2 at high pressures. *Physical Review B* **2008,** 78, (13), 134106.

31. Page, Y. L.; Saxe, P., Symmetry-general least-squares extraction of elastic data for strained materials from ab initio calculations of stress. *Physical Review B* **2002,** 65, (10), 104104.

32. Wu, Z. J.; Zhao, E. J.; Xiang, H. P.; Hao, X. F.; Liu, X. J.; Meng, J., Publisher's Note: Crystal structures and elastic properties of superhard IrN[sub 2] and IrN[sub 3] from first principles [Phys. Rev. B 76, 054115 (2007)]. *Physical Review B* **2007,** 76, (5), -.

33. Henkelman, G.; Uberuaga, B. P.; Jónsson, H., A climbing image nudged elastic band method for finding saddle points and minimum energy paths. *The Journal of chemical physics* **2000,** 113, (22), 9901-9904.

34. Emly, A.; Kioupakis, E.; Van der Ven, A., Phase Stability and Transport Mechanisms in Antiperovskite Li3OCl and Li3OBr Superionic Conductors. *Chemistry of Materials* **2013,** 25, (23), 4663-4670.

35. van de Walle, A.; Ceder, G., Automating first-principles phase diagram calculations. *J Phase Equilib* **2002,** 23, (4), 348-359.

36. Xiao, R.; Li, H.; Chen, L., Density Functional Investigation on Li2MnO3. *Chemistry of Materials* **2012,** 24, (21), 4242-4251.

37. Nye, J. F., *Physical properties of crystals*. Clarendon Press ;: 1985; p 391-397.

38. Usui, H.; Yoshioka, S.; Wasada, K.; Shimizu, M.; Sakaguchi, H., Nb-doped rutile TiO_2: a potential anode material for Na-ion battery. *ACS applied materials & interfaces* **2015,** 7, (12), 6567.

39. Wang, S.; Liu, J.; Sun, Q., New allotropes of Li2MnO3 as cathode materials with better cycling performance predicted in high pressure synthesis. *Journal of Materials Chemistry A* **2017,** 5, (32).

40. Guo, S.; Sun, Y.; Yi, J.; Zhu, K.; Liu, P.; Zhu, Y.; Zhu, G.; Chen, M.; Ishida, M.; Zhou, H., Corrigendum: Understanding sodium-ion diffusion in layered P2 and P3 oxides via experiments and first-principles calculations: a bridge between crystal structure and electrochemical performance. *Npg Asia Materials* **2016,** 8, (4).

41. Laks, D. B.; Ferreira, L. G.; Froyen, S.; Zunger, A., Efficient cluster expansion for substitutional systems. *Physical Review B Condensed Matter* **1992,** 46, (19), 12587.

42. Wolverton, C.; Zunger, A., First-principles prediction of vacancy order-disorder and intercalation battery voltages in Li x CoO 2. *Phys Rev Lett* **1998,** 81, (3), 606.

43. Persson, K.; Hinuma, Y.; Meng, Y. S.; Van der Ven, A.; Ceder, G., Thermodynamic and kinetic properties of the Li-graphite system from first-principles calculations. *Phys Rev B* **2010,** 82, (12), 125416.

44. Bj; ouml; Uuml, R.; Scheffler, L., Thermodynamics of the Heusler alloy Co2−xMn1+xSi: A combined density functional theory and cluster expansion study. *Phys.rev.b* **2009,** 79, (9), 4407.

45. Walle, A. V. D.; Asta, M., Self-driven lattice-model Monte Carlo simulations of alloy thermodynamic. *Modelling & Simulation in Materials Science & Engineering* **2002,** 10, (5), 521-538.

46. Van, d. V., A; Ceder, G., Vacancies in ordered and disordered binary alloys treated with the cluster expansion. *Physical Review B* **2005,** 71, (5).

47. Lee, E.; Persson, K. A., Structural and Chemical Evolution of the Layered Li-Excess Li x MnO 3 as a Function of Li Content from First-Principles Calculations. *Advanced Energy Materials* **2014,** 4, (15), 27-32.

48. Liu, J.; Wang, S.; Sun, Q., All-carbon-based porous topological semimetal for Li-ion battery anode material. *Proceedings of the National Academy of Sciences of the United States of America* **2017,** 114, (4), 651.

49. Zhou, F.; Cococcioni, M.; Marianetti, C. A.; Morgan, D.; Ceder, G., First-principles prediction of redox potentials in transition-metal compounds with LDA+U. *Physical Review B* **2005,** 70, (23), 35-40.

50. Wang, L.; Maxisch, T.; Ceder, G., Oxidation energies of transition metal oxides within the GGA + U framework. *Physical Review B* **2006,** 73, (19), 195107.

51. Zhou, F.; Cococcioni, M.; Marianetti, C. A.; Morgan, D.; Ceder, G., First-principles prediction of

redox potentials in transition-metal compounds withLDA+U. *Physical Review B* **2004,** 70, (23).
52. Li, Q.; Chen, J.; Fan, L.; Kong, X.; Lu, Y., Progress in electrolytes for rechargeable Li-based batteries and beyond. *Green Energy & Environment* **2016,** 1, (1), 18-42.

AUTHOR INFORMATION

*Corresponding Author: Qiang Sun, sunqiang@pku.edu.cn

ORCID

Qiang Sun: 0000-0003-3872-7267

Puru Jena: 0000-0002-2316-859X

Notes: The authors declare no competing financial interest.

TOC